Vibration suppression of suspended cables with three-to-one internal resonances via time-delay feedback

Vibration suppression of suspended cables with three-to-one internal resonances via time-delay feedback

Jian Peng[a,b,*], Yanan Li[a], Stefano Lenci[c], Xiangzhan Yang[d] and Lianhua Wang[d,*]

[a]School of Civil Engineering, Hunan University of Science and Technology, Xiangtan, Hunan 411201, PR China
[b]Hunan Provincial Key Laboratory of Structures for Wind Resistance and Vibration Control, Hunan University of Science and Technology, Xiangtan, Hunan 411201, PR China
[c]Department of Civil and Building Engineering and Architecture, Polytechnic University of Marche, Ancona 60131, Italy
[d]College of Civil Engineering, Hunan University, Changsha, Hunan 410082,China

ARTICLE INFO

Keywords:
suspended cable
time-delay feedback
internal resonance
vibration control
energy transfer

ABSTRACT

Based on the time-delay feedback control, the vibration suppression and energy transfer of suspended cables with three-to-one internal resonances are investigated. Initially, the nonlinear differential equation of motion for a suspended cable under time-delay feedback control is considered, and a discrete model is derived using the Galerkin method. Subsequently, the method of multiple scales is employed to perturbatively solve the discrete time-delay differential equation, determining the modulation equations around the first primary resonance. Steady-state and periodic solutions of the modulation equations are detected numerically. Numerical results indicate that the internal resonance enhances the nonlinear dynamical complexity of the controlled suspended cable. It is observed that the time delay and control gain affect the controlled system: in particular, an increase in control gain leads to a reduction in response amplitude. By adjusting the time delay and control gain, the critical excitation can be altered, an aspect that could be very useful from a pratical point of view. This research sheds light on the intricate dynamics of suspended cable and provides a theoretical foundation for designing more effective control strategies in engineering applications.

1. Introduction

Suspended cables are commonly used structural forms, widely applied in engineering projects such as bridges and cableways. Due to their high strength, large span, and lightweight advantages, suspended cables are increasingly gaining attention and application in modern constructions. On one hand, during operation, suspended cable systems often encounter a range of dynamic problems influenced by their inherent nonlinear characteristics and external excitation, such as resonance and amplitude magnification [1]. On the other hand, under the action of loads and in certain conditions, energy is mutually transferred between different structural elements of the suspended cable systems, involving multiple modes in actual vibrations and thereby inducing significant oscillations [2]. These issues can adversely affect the stability and safety of the suspended cable [3]. Understanding these dynamics is crucial for predicting and mitigating potential risks associated with large amplitude vibrations and ensuring the longevity and reliability of such structures in their service life.

Suspended cable is a complex geometrically nonlinear structure, encompassing both quadratic and cubic terms, which allows for a variety of phenomena that are not observable in the linear domain. If these nonlinearities and behaviors are not properly considered, they can pose a serious threat to the safety and stability of engineering structures [4]. Conversely, if their nonlinear characteristics are appropriately harnessed, not only can potential dangers be avoided, but new avenues for the application of suspended cable in engineering can also be discovered.

Under external excitation, suspended cable may exhibit modal coupling and energy transfer between different modes, particularly through the internal resonance phenomena, which holds a significant place in the study of multimodal dynamics. Because of its importance, numerous scholars have conducted in-depth investigations: Rao et al. [5] studied the internal and nonlinear response of a cable under periodic excitation, considering both internal and external resonance, and studied the effect of cable sag on the solutions and their stability through internal resonance. Lee and Perkins [2] employed a two-degree-of-freedom model to investigate the nonlinear vibration of suspended

*Corresponding author
pengjian@hnu.edu.cn (J. Peng); Lhwang@hnu.edu.cn (L. Wang)

cable with 2:1 internal resonance under planar excitation. Rega et al. [6, 7] studied the nonlinear vibrations of a four-degree-of-freedom model of a suspended cable under multiple internal resonance conditions, including both in-plane and out-of-plane components. Zhao et al. [8] analyzed the two-modal nonlinear response of a suspended cable under primary resonance and further explored three-to-one internal resonance. Srinil et al. [9, 10] conducted a parametric study on the dynamics of multimode resonances induced by planar 2:1 internal resonance in nonlinear, finite-amplitude, and free vibrations of horizontal/inclined cable systems. Kang et al. [11] established a nonlinear dynamic model for the shallow arch and dual cables of a cable-stayed bridge and analyzed the in-plane 1:1:1 internal resonance under external primary and subharmonic resonances. Hui et al. [12] investigated the internal resonance phenomena of a suspended bridge structure with inclined main cables based on a six-degree-of-freedom sectional model. Xu et al. [13] studied the internal resonance and vertical vibrations of the bridge deck of a suspension bridge composed of spatially inclined main cables and suspenders through a continuum model. Zhao et al. [14] researched the 2:1 internal resonance nonlinear dynamics of suspended cables in thermal environments under periodic excitation. Peng et al. [15] explored the time-delay dynamics of the MR damper-cable system with 1:1 internal resonances. Su et al. [16] modeled and studied the energy transfer in the coupled nonlinear response of a 1:1 internally resonant cable system with a tuned mass damper. Sun et al. [17] explored the multiple internal resonances and their modal interaction processes of a cable-stayed bridge physical model through experiments and finite element model. These comprehensive studies enhance our understanding of the complex behaviors of suspended cables.

In recent years, various methods and control systems have been developed to mitigate the large amplitude vibrations of suspended cables, and considerable theoretical and experimental research has been conducted in this field. Generally, these can be categorized into aerodynamic measures [18, 19], auxiliary cable measures [20, 21], and vibration control methods using dampers (including passive control [22], active control [23], semi-active control [24], etc.). Among these, the damper control method is the most widely applied in engineering practice. However, recent studies have shown that the vibration control methods currently employed in engineering are primarily suited for single-mode control, with a narrow effective frequency range and weak robustness, making it challenging to suppress the higher-order multimodal nonlinear vibrations of large-span cable structures [25]. To address this issue, the concept of time-delay feedback control has been introduced [26]. Characterized by its broad frequency band and efficient damping performance, it effectively enhances the vibration reduction capability and stability of engineering structures under various dynamic conditions, and thus, has been widely applied [27–29].

Continuing and further developing this important research field, the novelty and the main contribution of this work is primarily centered on the vibration control of suspended cables experiencing a 3:1 internal resonance, utilizing time-delay feedback. More specifically, in Section 2 the nonlinear dynamic equations for suspended cables under the influence of time-delay vibration control are reported and then discretized via the Galerkin method. In Section 3, the perturbative solution of the derived differential equations is obtained using the method of multiple scales, with steady-state and periodic solutions being sought through the employment of the Newton-Raphson and shooting methods. In Section 4, numerical simulations are presented, where the internal resonance response of the controlled suspended cable is analyzed in depth, and the efficacy and mechanisms of time-delay feedback control in mitigating complex vibrations and enhancing the structural stability and safety of the cable are verified. Conclusion are summarized in Section 5.

2. Mathematical model

The considered suspended cable is schematically illustrated in Figure 1a. The origin O of the reference system is located on left side. Assuming that the cable is homogeneous, has negligible bending stiffness and considering only the in-plane behaviour, the nonlinear equation of motion is [7]

$$m\ddot{v} + 2c\dot{v} - Hv'' - \frac{EA}{L}(y'' + v'')\left[u_c + \int_0^L (y'v' + \frac{1}{2}v'^2)dx\right] = F(x,t), \tag{1}$$

where m is the mass per unit length c is the damping coefficient; E is the elastic modulus; A is the cross-sectional area; L is the span; H is the horizontal tension ($H = mgL^2/8b, H \leq EA$); b is the sag; g is the acceleration due to gravity; u_c is the longitudinal displacement applied to the right end support; $F(x,t) = P(x)\cos(\Omega t)$ is the external excitation; Ω is the frequency of the external excitation; $P(x)$ is the distribution function of the external excitation.

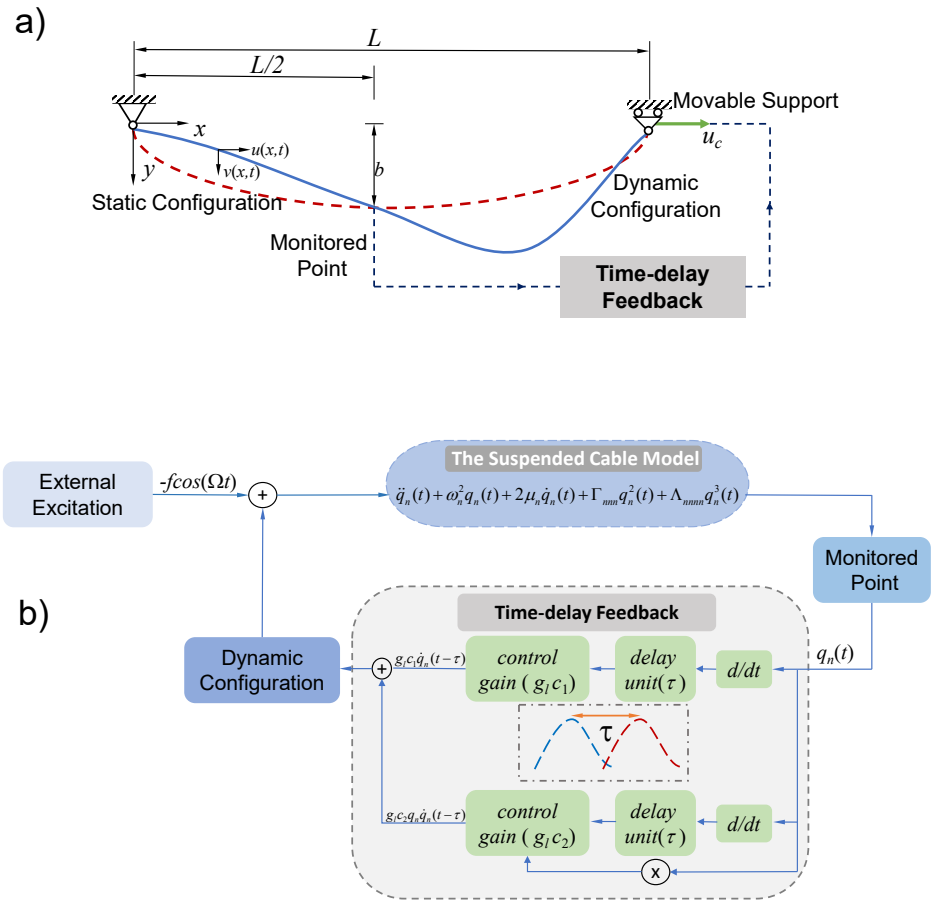

Figure 1: The schematic of the controlled suspended cable and operating system. a) Controlled suspended cable; b) Schematic diagram of the whole system.

We assume that the sag ratio of the suspended cable is small ($b/L < 1/8$), so its shape can be described as a parabola

$$y(x) = 4b\left[x/L - (x/L)^2\right].$$

The linear time-delayed feedback strategy is adopted for vibration control, namely

$$u_c(t) = g_l \dot{v}(x_c, t-\tau),$$

where g_l is the control gain, τ is the time delay, and $x_c = L/2$ is the position of the monitored point used drive the control. This latter is schematically illustrated in Figure 1b.

Let us introduce the dimensionless parameters

$$x^* = x/L, \quad y^* = y/L, \quad v^* = v/L, \quad \alpha = EA/H,$$
$$P^* = PL/H, \quad t^* = t\sqrt{g/8b}, \quad \Omega^* = \Omega\sqrt{8b/g},$$
$$c^* = (c/m)\sqrt{8b/g}, \quad {g_l}^* = g_l/L, \quad \tau^* = \tau\sqrt{g/8b}.$$

After non-dimensionalization, the Eq. (1) can be expressed as

$$\ddot{v} + 2c\dot{v} - v'' - \alpha(y'' + v'')\left[u_c + \int_0^1 (y'v' + \frac{1}{2}v'^2)dx\right] = P(x)\cos(\Omega t), \tag{2}$$

where the stars are omitted for simplicity.

Using the Galerkin method to discrete Eq. (2), the dimensionless displacement is assumed as

$$v(x,t) = \sum_{n=1}^{\infty} q_n(t)\phi_n(x), \tag{3}$$

where $\phi_n(x)$ are the mode shape function and $q_n(t)$ their amplitudes. Substituting Eq. (3) into Eq. (2), and integrating on the spatial domain [0, 1], we obtain

$$\begin{aligned}&\ddot{q}_n(t) + \omega_n^2 q_n(t) + 2\mu_n\dot{q}_n(t) + \sum_{i,j=1}^{\infty}\Gamma_{nij}q_i(t)q_j(t) + \sum_{i,j.k=1}^{\infty}\Lambda_{nijk}q_i(t)q_j(t)q_k(t)\\ &+ \sum_{i=1}^{\infty} g_l c_{1,ni}\dot{q}_i(t-\tau) + \sum_{i,j=1}^{\infty} g_l c_{2,nij}q_i(t)\dot{q}_j(t-\tau) = f_n\cos(\Omega t),\end{aligned} \tag{4}$$

where,

$$\Gamma_{nij} = -\alpha\int_0^1\left[\phi_j''(x)\int_0^1\phi_i'(x)y'\,dx\right]\phi_n(x)\,dx - \frac{1}{2}\alpha\int_0^1\left[y''\int_0^1\phi_j'(x)\phi_i'(x)\,dx\right]\phi_n(x)\,dx,$$

$$\Lambda_{nijk} = -\frac{1}{2}\alpha\int_0^1\left[\phi_j''(x)\int_0^1\phi_k'(x)\phi_i'(x)\,dx\right]\phi_n(x)\,dx,$$

$$f_n = -\int_0^1 P(x)\phi_n(x)dx, \quad \mu_n = \int_0^1 c\phi_n^2(x)dx,$$

$$c_{1,ni} = -\alpha\phi_i(x_c)\int_0^1 y''\phi_n(x)\,dx, \quad c_{2,nij} = -\alpha\phi_j(x_c)\int_0^1\phi_i''(x)\phi_n(x)\,dx.$$

Ignoring the effects of damping, external excitation, control and nonlinear terms, we can obtain the symmetric and anti-symmetric mode shapes and their frequencies for a suspended cable.

The symmetric mode shapes function of the suspended cable are given by [30]:

$$\phi_n(x) = \xi_n\left[1 - \cos(\omega_n x) - \tan\left(\frac{\omega_n}{2}\right)\sin(\omega_n x)\right], (n = 1, 3, 5, ...). \tag{5}$$

In Eq. (5), the coefficients ξ_n can be determined based on the mode normalization condition $\int_0^1\phi_n^2(x)dx = 1$. The symmetric frequencies ω_n (n = 1,3,5,...) are obtained by solving the following transcendental equation

$$\tan\left(\frac{\omega_n}{2}\right) = \frac{\omega_n}{2} - \frac{1}{2\lambda^2}\omega_n^3, \tag{6}$$

where $\lambda^2 = EA/mgl(8d)^3$, $d = b/l$ being the sag-to-span ratio, which is small to have that (1) is reliable.

The anti-symmetric mode shapes and frequencies are given by

$$\phi_n(x) = \sqrt{2}\sin(n\pi x), \quad \omega_n = n\pi, \quad n = 2, 4, 6, ... \tag{7}$$

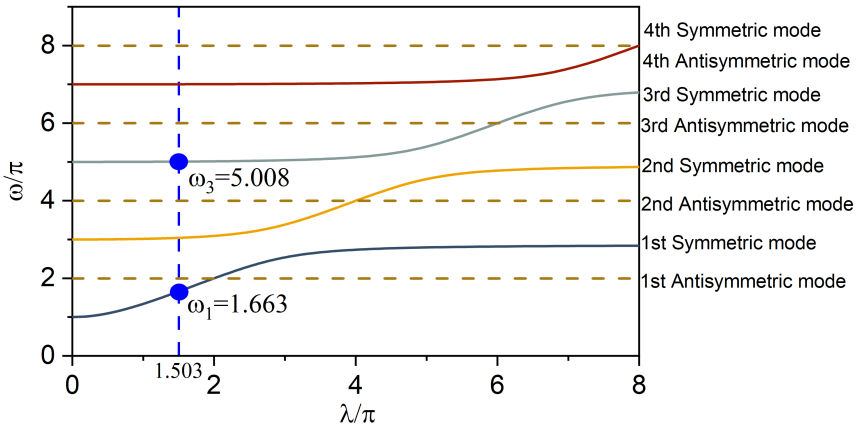

Figure 2: The nondimensional natural frequencies of the suspended cable

3. Perturbation analysis

Figure 2 illustrates the dependence of the natural frequencies ω_n on the elastic-geometric parameter λ. Solid lines represent symmetric modes (see Eq. (6)), while dashed lines denote antisymmetric modes, which, according to Eq. (7), are independent of λ. It is evident that different paths of symmetric modes converge to $(n+2)\pi$ for $\lambda \to \infty$.

In this paper, the main focus is on the nonlinear behavior of the first symmetric mode and the third symmetric mode, which exhibit a 3:1 internal resonance ($\omega_3 \approx 3\omega_1$) when $\lambda/\pi = 1.503$, as shown in Fig. 2. It is further assumed that the first symmetric mode is in primary resonance ($\Omega \approx \omega_1$) with the external excitation.

A small quantity ε is introduced to rescale the coefficients of each term in Eq. (4) as

$$\mu_n \approx \varepsilon^2 \mu_n, \quad f_n \approx \varepsilon^2 f_n, \quad \Gamma_{nij} = \varepsilon \Gamma_{nij}, \quad \Lambda_{nijk} = \varepsilon^2 \Lambda_{nijk}, \quad g_l = \varepsilon^2 g_l.$$

Then, the solution $q_n(t;\varepsilon)$ is sought after in the form

$$q_n(t,\varepsilon) = \sum_{i=0}^{2} \varepsilon^i q_{ni}(T_0, T_1, T_2), \tag{8}$$

where $T_i = \varepsilon^i t$. Substituting in Eq. (4), expanding, and setting the coefficients of the same powers of ε equal to zero, we obtain the following sequences of linear differential equations:

$O(\varepsilon^0)$

$$D_0^2 q_{n0} + \omega_n^2 q_{n0} = 0, \tag{9}$$

$O(\varepsilon^1)$

$$D_0^2 q_{n1} + \omega_n^2 q_{n1} = -2D_0 D_1 q_{n0} - \sum_{i=1}^{\infty}\sum_{j=1}^{\infty} \Gamma_{nij} q_{i0} q_{j0}, \tag{10}$$

$O(\varepsilon^2)$

$$\begin{aligned} D_0^2 q_{n2} + \omega_n^2 q_{n2} = &-2D_0 D_2 q_{n0} - D_1^2 q_{n0} - 2D_0 D_1 q_{n1} - 2\mu_n D_0 q_{n0} - \sum_{i=1}^{\infty}\sum_{j=1}^{\infty} \Gamma_{nij}(q_{i0} q_{j1} + q_{i1} q_{j0}) \\ &- \sum_{i=1}^{\infty}\sum_{j=1}^{\infty}\sum_{k=1}^{\infty} \Lambda_{nijk} q_{i0} q_{j0} q_{k0} - g_l c_1 D_0 q_{n0}(t-\tau) - g_l c_2 q_{n0} D_0 q_{n0}(t-\tau) + f_n \cos(\Omega t). \end{aligned} \tag{11}$$

Solving Eq. (9) yields

$$q_{n0} = A_n\left(T_1, T_2\right) e^{i\omega_n T_0} + cc, \tag{12}$$

where cc represents the complex conjugate of the preceding terms. By substituting Eq. (12) into Eq. (10) and eliminating the secular terms, it can be concluded that A_n is independent of T_1, $D_1 A_n = 0$, which gives us

$$D_0^2 q_{n1} + \omega_n^2 q_{n1} = -\sum_{i=1}^{\infty}\sum_{j=1}^{\infty}\Gamma_{nij}(A_i A_j e^{i(\omega_i+\omega_j)T_0} + A_i \bar{A}_j e^{i(\omega_i-\omega_j)T_0}) + cc. \tag{13}$$

Therefore, we can obtain the solution of Eq. (10) as

$$q_{n1} = -\sum_{i=1}^{\infty}\sum_{j=1}^{\infty}\Gamma_{nij}\left(\frac{A_i A_j e^{i(\omega_i+\omega_j)T_0}}{\omega_n^2-(\omega_i+\omega_j)^2} + \frac{A_i \bar{A}_j e^{i(\omega_i-\omega_j)T_0}}{\omega_n^2-(\omega_i-\omega_j)^2}\right) + cc. \tag{14}$$

It is assumed that the denominators do not vanish, i.e. $\omega_n^2 \neq (\omega_i+\omega_j)^2$ and $\omega_n^2 \neq (\omega_i-\omega_j)^2$.

By introducing the detuning parameters σ_1 and σ_2, we can quantitatively describe the closeness between Ω and ω_1, as well as the closeness between ω_3 and $3\omega_1$:

$$\Omega = \omega_1 + \varepsilon^2\sigma_1 \qquad \omega_3 = 3\omega_1 + \varepsilon^2\sigma_2 \tag{15}$$

By substituting Eq. (12) and Eq. (14) into Eq. (11), in order to eliminate the secular term, the following modulation equations must be satisfied

$$2i\omega_1\left(D_2 A_1 + \mu_1 A_1\right) = \gamma_{11}A_1^2\bar{A}_1 + \gamma_{13}A_1 A_3\bar{A}_3 + \delta_1 A_3\bar{A}_1^2 e^{i\varepsilon^2\sigma_3 T_0} + \frac{1}{2}f_1 e^{i\sigma_1 T_2} + i\omega_1 g_{l1}A_1 e^{-i\omega_1\tau} = 0, \tag{16}$$

$$2i\omega_3\left(D_2 A_3 + \mu_3 A_3\right) = \gamma_{33}A_3^2\bar{A}_3 + \gamma_{31}A_3 A_1\bar{A}_1 + \delta_3 A_1^3 e^{-i\sigma_3 T_2}, \tag{17}$$

where $T_2 = \varepsilon^2 T_0$ is used and where

$$\begin{aligned}
\gamma_{ij} &= \sum_{n=1}^{\infty}\left[(\Gamma_{iin}+\Gamma_{ini})\left(\frac{2\Gamma_{nii}}{\omega_n^2} + \frac{\Gamma_{nii}}{\omega_n^2-4\omega_i^2}\right) + 3\Lambda_{iiii}\right] \quad (i=j)\\
\gamma_{ij} &= \sum_{n=1}^{\infty}\left[(\Gamma_{iin}+\Gamma_{ini})\frac{2\Gamma_{nii}}{\omega_n^2} + (\Gamma_{ijn}+\Gamma_{inj})(\Gamma_{nij}+\Gamma_{nji})\left(\frac{1}{\omega_n^2-(\omega_i+\omega_j)^2} + \frac{1}{\omega_n^2-(\omega_i-\omega_j)^2}\right)\right]\\
&\quad + 2(\Lambda_{ijji}+\Lambda_{ijij}+\Lambda_{iijj}) \quad (i\neq j)\\
\delta_3 &= \sum_{n=1}^{\infty}\left[(\Gamma_{31n}+\Gamma_{3n1})\frac{\Gamma_{n11}}{\omega_n^2-4\omega_1^2}\right] + \Lambda_{3111}\\
\delta_1 &= \sum_{n=1}^{\infty}\left[\left(\Gamma_{13n}+\Gamma_{1n3}\right)\frac{\Gamma_{n11}}{\omega_n^2-4\omega_1^2} + \left(\Gamma_{11n}+\Gamma_{1n1}\right)\frac{\left(\Gamma_{n13}+\Gamma_{n31}\right)}{\omega_n^2-\left(\omega_3-\omega_1\right)^2}\right] + \left(\Lambda_{1311}+\Lambda_{1131}+\Lambda_{1113}\right)\\
g_{l1} &= g_l c_1.
\end{aligned} \tag{18}$$

To study the stability of the steady-state solution, we also introduce a Cartesian coordinate transformation

$$A_n(T_2) = \frac{1}{2}[p_n(T_1) - iq_n(T_2)]e^{i\nu_n T_2}, \quad n = 1, 3. \tag{19}$$

By substituting in Eqs. (16) and (17) and separating the real and imaginary parts, we obtain

$$\begin{aligned}
p_1' = &-\nu_1 q_1 - \mu_1 p_1 - \frac{1}{8\omega_1}\gamma_{11}q_1(p_1^2+q_1^2) - \frac{1}{8\omega_1}\gamma_{13}q_1(p_3^2+q_3^2)\\
&- \frac{1}{8\omega_1}\delta_1[q_3(p_1^2-q_1^2) - 2p_1 q_1 p_3] - \frac{1}{2}g_{l1}p_1\cos(\omega_1\tau) + \frac{1}{2}g_{l1}q_1\sin(\omega_1\tau),
\end{aligned} \tag{20}$$

Table 1
Cable geometry and material properties parameters

Density ρ (kg m^{-3})	Elastic modulus E (Pa)	Cross-sectional area A (m^2)	Span L (m)	Damping ratio μ_1	μ_3	Aspect ratio d
7800	2×10^{11}	7.069×10^{-2}	200	0.005	0.006	0.015

$$\begin{aligned} q_1' =& \nu_1 p_1 - \mu_1 q_1 + \frac{1}{8\omega_1}\gamma_{11} p_1 (p_1^2 + q_1^2) + \frac{1}{8\omega_1}\gamma_{13} p_1 (p_2^2 + q_2^2) - \frac{1}{2} g_{l1} p_1 \sin(\omega_1 \tau) \\ &+ \frac{1}{8\omega_1}\delta_1 [p_3 (p_1^2 - q_1^2) + 2 p_1 q_1 q_3] - \frac{1}{2} g_{l1} q_1 \cos(\omega_1 \tau) + \frac{1}{2\omega_1} f_1, \end{aligned} \tag{21}$$

$$\begin{aligned} p_3' =& -\nu_3 q_3 - \mu_3 p_3 - \frac{1}{8\omega_3}\gamma_{31} q_3 (p_1^2 + q_1^2) - \frac{1}{8\omega_3}\gamma_{33} q_3 (p_3^2 + q_3^2) \\ &- \frac{1}{8\omega_3}\delta_3 (q_1^3 - 3 p_1^2 q_1) - \frac{1}{2} g_{l1} p_3 \cos(\omega_3 \tau) + \frac{1}{2} g_{l1} q_3 \sin(\omega_3 \tau), \end{aligned} \tag{22}$$

$$\begin{aligned} q_3' =& \nu_3 p_3 - \mu_3 q_3 + \frac{1}{8\omega_3}\gamma_{31} p_3 (p_1^2 + q_1^2) + \frac{1}{8\omega_3}\gamma_{33} p_3 (p_3^2 + q_3^2) \\ &+ \frac{1}{8\omega_3}\delta_3 (p_1^3 - 3 p_1 q_1^2) - \frac{1}{2} g_{l1} p_3 \sin(\omega_3 \tau) - \frac{1}{2} g_{l1} q_3 \cos(\omega_3 \tau), \end{aligned} \tag{23}$$

where $\nu_1 = \sigma_3$ and $\nu_2 = 3\sigma_3 - \sigma_1$, and where prime means derivative with respect to T_2.

The stability is determined by investigating the eigenvalues of the Jacobian matrix of linearized version of Eqs. (20)-(23) around the considered solutions, that are equilibrium points of (20)-(23), i.e. those satisfying $p_1' = q_1' = p_3' = q_1' = 0$, and correspond to periodic solutions in the original system (2). The real parts of the eigenvalues determine the stability of the system: (a) If the real parts of all the eigenvalues are negative, then the equilibrium point is asymptotically stable. (b) If at least one eigenvalue has a positive real part, then the equilibrium point is unstable. (c) If all the real parts of the eigenvalues are non-positive, and at least one eigenvalue has a real part equal to zero, then the system may exhibit boundary stability and further analysis is required.

4. Equilibrium solutions and stability

With the aim of illustrating the nonlinear dynamics of the considered system, in this section, using the parameters of Tab. 1, that corresponds to $\lambda = 1.503\pi$, the Eqs. (20)-(23) are integrated numerically by the Runge-Kutta method and the Newton-Raphson iteration and the shooting methods are used to detect the equilibrium and periodic points (including the unstable ones).

4.1. Effect of the control delay

In this section, we are aimed at investigating the effect of the control delay. We fix the control gain $g_{l1} = 0.248$, the external excitation amplitude $f = 0.0025$ and consider three different time-delays, $\tau = \pi/35, \pi/64, \pi/128$.

Figure 3 presents the time-history of the first and third modes for $\sigma_1 = -0.125$, encompassing the uncontrolled state, the active control state without time delay, and the time-delay control under two different parameter settings. It is seen that in the uncontrolled state, the system exhibits large amplitude periodic motions. After the application of the active control, i.e. $u_c = g_l \dot{v}$, the system's vibrations are significantly reduced, demonstrating the effectiveness of the control strategy. The introduction of time-delay feedback control not only achieves vibration suppression but also enhances the damping efficiency compared to the active control without time delay, particularly in the control of a_3. In fact, it is evident that as the time delay increases from $\pi/128$ to $\pi/35$, the system's amplitude gradually reduces, demonstrating a pronounced effect of the control. It is necessary to underline that this conclusion is valid only for $\sigma_1 = -0.125$, and cannot be generalized.

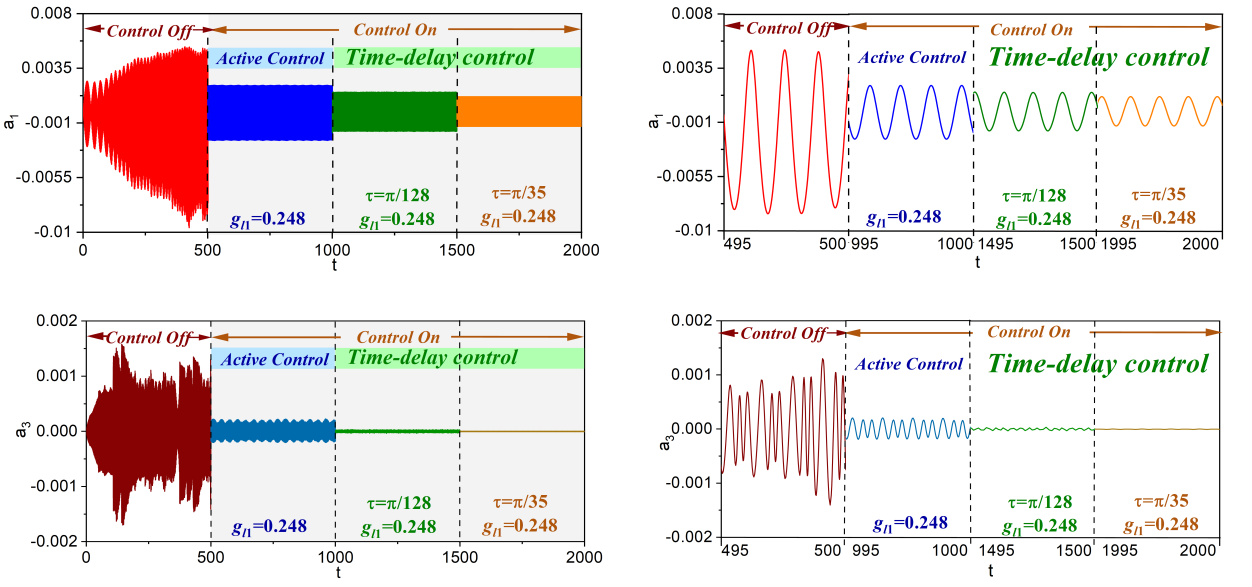

Figure 3: The time-histories of the first and third modes under different time delay

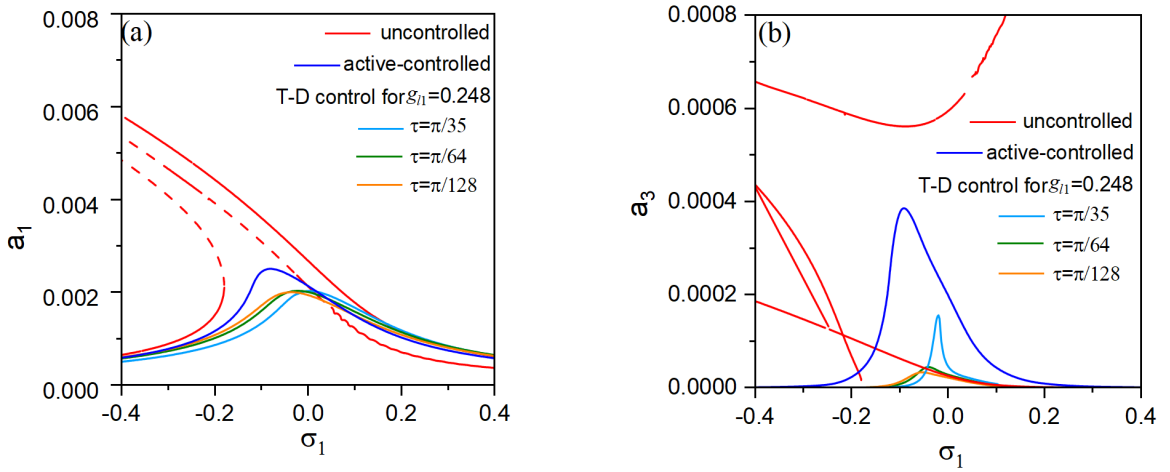

Figure 4: Amplitude-frequency response curves of the suspended cable at different time delay, (a) $a_1(\sigma_1)$, (b) $a_3(\sigma_1)$

Subsequently, we extend the previous results to different values of σ_1, and see the effect of the external frequency in a neighborhood of the primary resonance of the first symmetric mode ($\Omega \approx \omega_1$).

Figure 4 illustrates the amplitude-frequency curves for the three considered time-delay values. Solid lines represent stable solutions and dashed lines unstable ones. The red curves denote the maximum amplitudes of a_1 and a_3 under an uncontrolled condition, consistent with the scenarios described in [31] and [32]. The blue curves show a_1 and a_3 under active control without delay, while the others corresponds to the three considered values of the delay.

As expected, the first mode, being directly excited, displays a larger response amplitude a_1, whereas the third mode amplitude a_3 remains smaller, although a portion of energy is transferred to it through 3:1 internal resonance

and although for the large delay there is a marked peak in the $a_3(\sigma_1)$ curve. Looking at the vertical scales of the Figs. 4(a) and 4(b) we see that, on average, a_1 is one order of magnitude larger than a_3.

The second point to be highlighted is the softening behaviour of the first mode, which is clearly visible for the uncontrolled case, but also for the controlled one without time delay.

Regarding vibration suppression, it is clear that the time delay τ does not change the peak amplitude of the first mode, and on the left of the peak the amplitude decreases by increasing τ, while on the right of the peak it very slightly increases. The conclusion is that τ has a different effect, depending on the value of the excitation frequency. The peak frequency is slightly changed, but to a minor extent and not enough to be relevant for applications. For decreasing τ there is a decrement in the amplitude of the third mode, that is initially relevant although this mode has only small amplitudes.

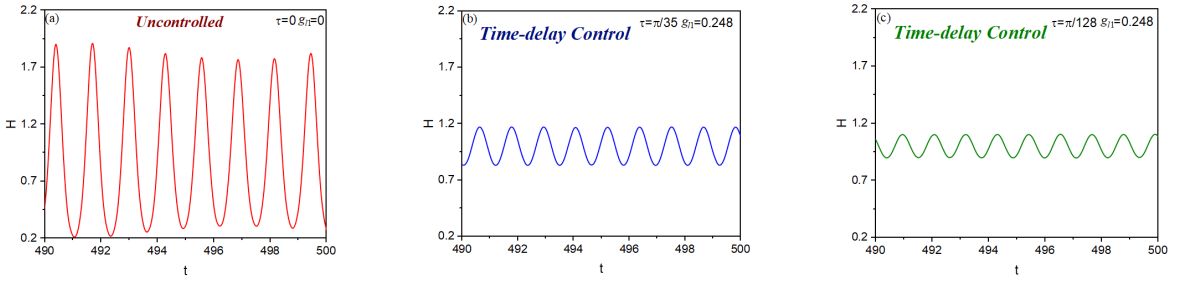

Figure 5: Horizontal tension diagrams under different time delay, (a) uncontrolled, (b) $\tau = \pi/35$, (c) $\tau = \pi/128$, $g_{l1} = 0.248$, $\Omega \approx \omega_1$

Due to the negligibile stiffness in compression, the total tension in the cable must be greater than zero to validate the proposed approach. The dimensionless horizontal tension H_T is

$$H_T = 1 + \alpha \int_0^1 (y'v' + \frac{1}{2}v'^2)dx. \tag{24}$$

Figure 5 depicts the time-history curves of the force for the first mode. As desired, in all cases, the horizontal tension is consistently positive. According to the expression for Eq. (24), it is evident that the magnitude of horizontal tension is closely related to the system displacement. Consequently, with the application of time-delay feedback control and the associated reduction of the displacements, the oscillating part of horizontal tension decreases accordingly. The variations of the force under different parameters could be exploited and thus beneficial for design optimization, ensuring that the cable meets the expected mechanical performance requirements under various operating conditions.

While the previous simulations refer to fixed values of τ, Figs. 6 and 7 illustrate the "continuous" variation of a_1 or a_3 with time delay τ and σ_1, and report only stable solutions. The color variation in the figure represents the amplitude, with warmer colors typically indicating higher amplitudes. The presence of multiple peaks indicates complex dynamical changes in the system, suggesting a strong interaction due to variations in time delay. From Fig. 6(b) it can be observed that a_1 exhibits a periodic pattern as a function of τ, and that it is very large only around the perfect resonance $\sigma_1 = 0$.

In comparison to a_1, the variation pattern of a_3 with respect to the time delay exhibits a more distinct periodicity, showing that for certain value of τ the third mode amplitude a_3 almost vanishes for all values of σ_1.

4.2. Effect of the control gain

In this section we fixed the time delay $\tau = \pi/35$, the external excitation $f = 0.0025$, and consider different control gains ($g_{l1} = 0.124, 0.198, 0.248$), still in the case of primary resonance of the first-order symmetric mode ($\Omega \approx \omega_1$).

Figure 8 illustrates the time-history for $\sigma_1 = -0.2$. It can be seen that the vibration is effectively reduced with the application of active control. Furthermore, by considering time-delay feedback control, the vibration of the suspended cable is further mitigated, particularly for a_3.

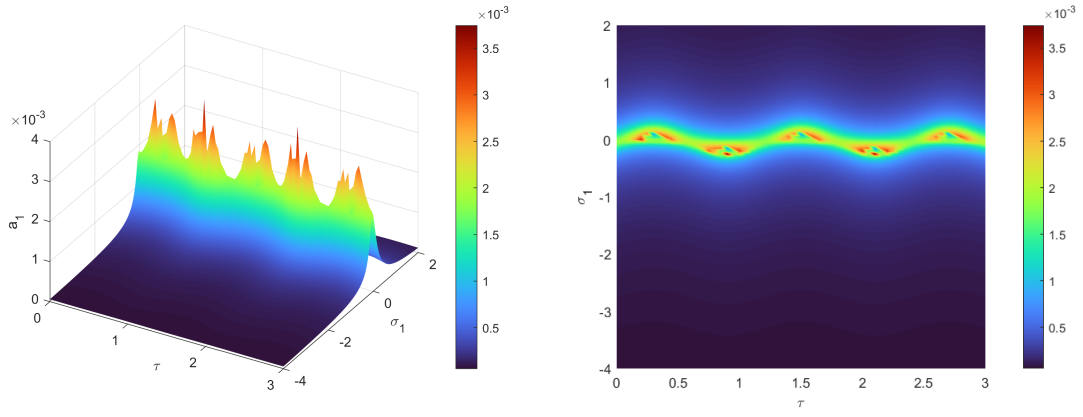

(a) The 3-D surface map (b) The 2-D contour map of a_1

Figure 6: The trend of the first order resonance amplitude with the variation of τ and σ_1 ($g_{l1} = 0.248$)

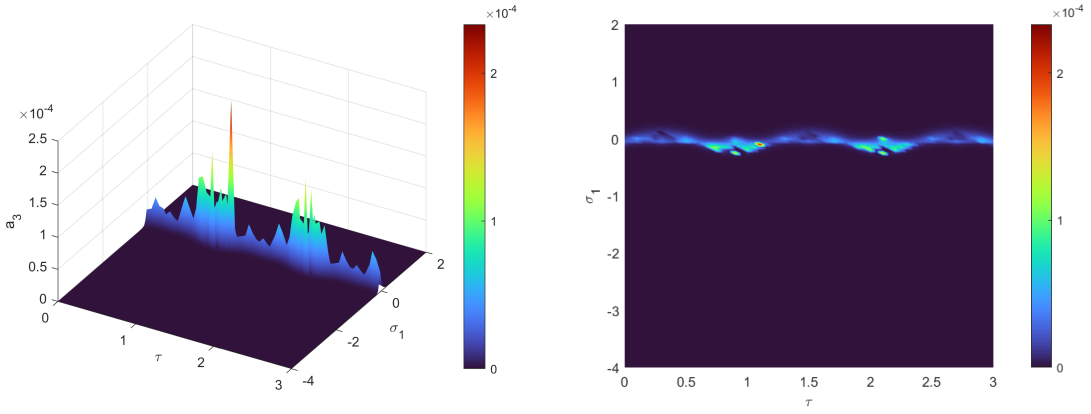

(a) The 3-D surface map (b) The 2-D contour of a_3

Figure 7: The trend of the third order resonance amplitude with the variation of τ and σ_1 ($g_{l1} = 0.248$)

Figure 9 presents the amplitude-frequency response curves. Again, solid lines indicate stable solutions, dashed lines indicate unstable solutions, red represents the uncontrolled state and blue indicates the active controlled state. In these scenarios, a_1 remains significantly larger than a_3. It is observed that, as the control gain increases from $g_{l1} = 0.124$ to $g_{l1} = 0.248$, the amplitude gradually decreases, demonstrating effectiveness in vibration suppression.

Figure 10 depicts the time-histories of the force for the first mode. As the control gains increase, the force always remains positive, as requested, and also gradually decreases its oscillation amplitude.

Figures 11 and 12 presents the "continuous" variation of the amplitude ratio a_1 or a_3 with control gain g_{l1} and detuning parameter σ_1 at a time delay $\tau = \pi/35$. The figure shows the presence of two peaks for a_1 and a unique sharp peak for a_3 around the uncontrolled $g_{l1} = 0$ and perfectly resonant $\sigma_1 = 0$ case. This means that, apart from a neighborhood of these peaks, the control is always able to reduce the response amplitude, and thus it is overall effective.

4.3. Effect of the excitation amplitude

Figure 13 presents the amplitudes of a_1 and a_3 for varying excitation amplitude f, with the other parameters kept fixed. When the gain is small (Fig. 13(a)) and when the external excitation amplitude is small, multiple solutions exist. The system response amplitude increases with the increase of external excitation, with the first-order modal amplitude being significantly larger than that of the third-order one. The unstable solutions vanish as the control gain increases

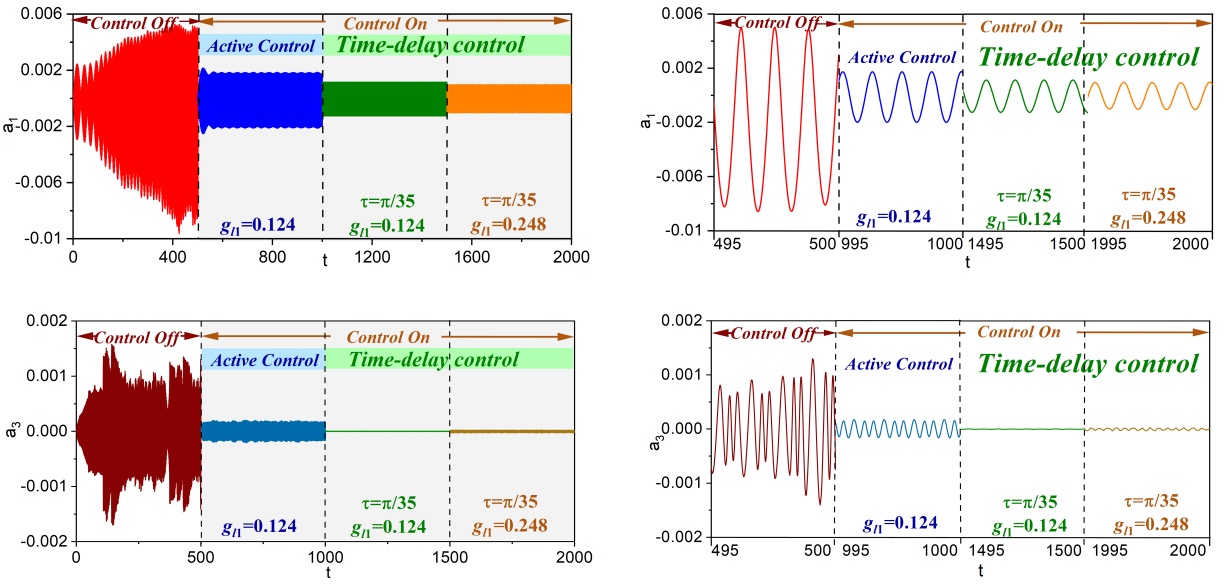

Figure 8: The time-history curves of the first mode under different control gains

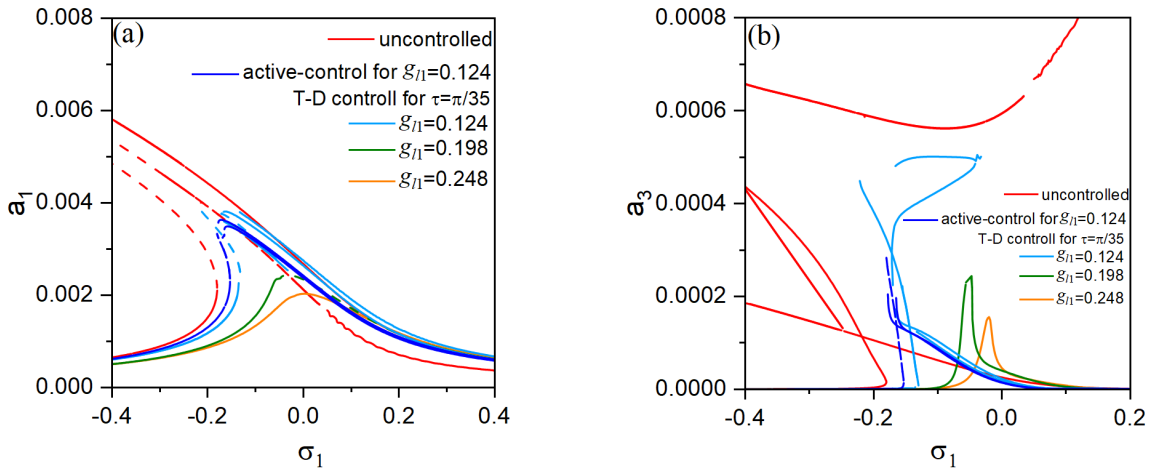

Figure 9: Amplitude-frequency response curves of the suspended cable at different control gains, (a) $a_1(\sigma_1)$, (b) $a_3(\sigma_1)$

(Fig. 13(b)). Therefore, by precisely adjusting the control gain and the external excitation amplitude, the multivalued solution situation can be effectively avoided.

5. Conclusions

In this study, we explored vibration suppression suspended cables, considering simultaneous occurrences of primary resonance and 3:1 internal resonance in the system. Utilizing the method of multiple scales, we obtained the modulation equations for the primary resonance of the first and third modes and conducted an in-depth numerical analysis of the internal resonance. Through amplitude-frequency curves, force-frequency curves, displacements time-history and horizontal tension diagrams, as well as 3-D surface map of τ-σ_1-a with a control gain $g_{l1} = 0.248$ and

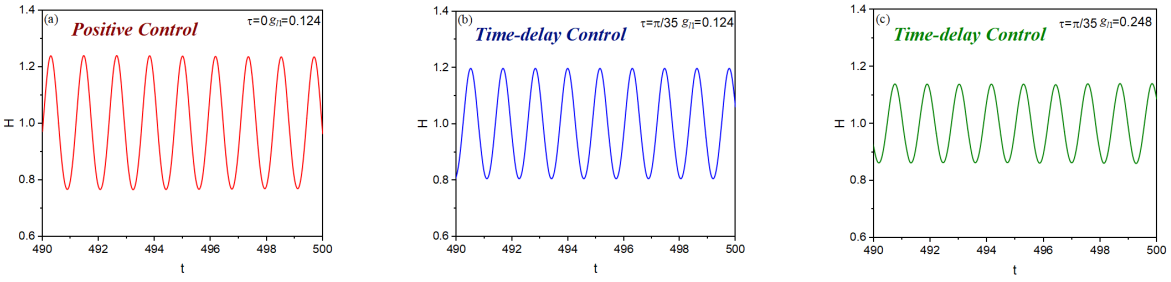

Figure 10: Horizontal tension diagrams under different control gains, (a) positive control, (b) $g_{l1} = 0.124$, (c) $g_{l1} = 0.248$, $\tau = \pi/35$, $\Omega \approx \omega_1$

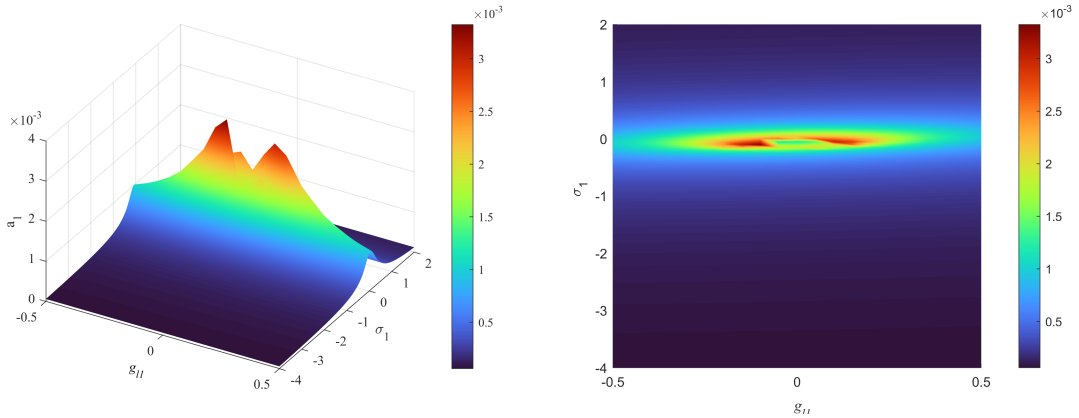

(a) The 3-D surface map (b) The 2-D contour map of a_3

Figure 11: The trend of the 1st-order resonance amplitude with the variation of g_{l1} and σ_1 ($\tau = \pi/35$)

g_{l1}-σ_1-a at a time delay $\tau = \pi/35$, we thoroughly examined the steady-state response and stability of the controlled suspended cable, analyzing the control effects under different parameters.

The summarized research findings are as follows:

1. The occurrence of internal resonance between modes made the nonlinear behavior of the controlled suspended cable more complex;
2. Time delay and control gain had a certain impact on the controlled system. The effect of τ varies for different value of g_{l1} and for different values of σ_1. An increase in control gain within a specific range resulted in a reduction in response amplitude, indicating a significant control effect;
3. Therefore, the application of time-delay control technology effectively suppressed the nonlinear vibration characteristics of the suspended cable. By selecting appropriate time delay and control gain, satisfactory control effects can be achieved.

Acknowledgements

The study was supported by the National Natural Science Foundation of China (Grant No.52078210) and Provincial Natural Science Foundation of Hunan (Grant No.2023JJ60527). The work of Prof. Lenci has been partially done within his belonging to the “Gruppo Nazionale per la Fisica Matematica", and within the “DICEA-Dipartimento di Eccellenza" project funded by Italian MUR.

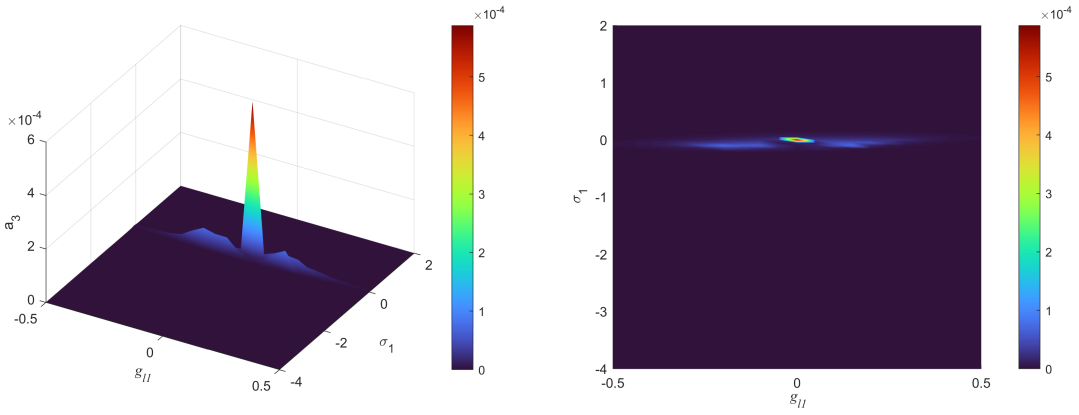

(a) The 3-D surface map (b) The 2-D contour map of a_3

Figure 12: The trend of the 3rd-order resonance amplitude with the variation of g_{l1} and σ_1 ($\tau = \pi/35$)

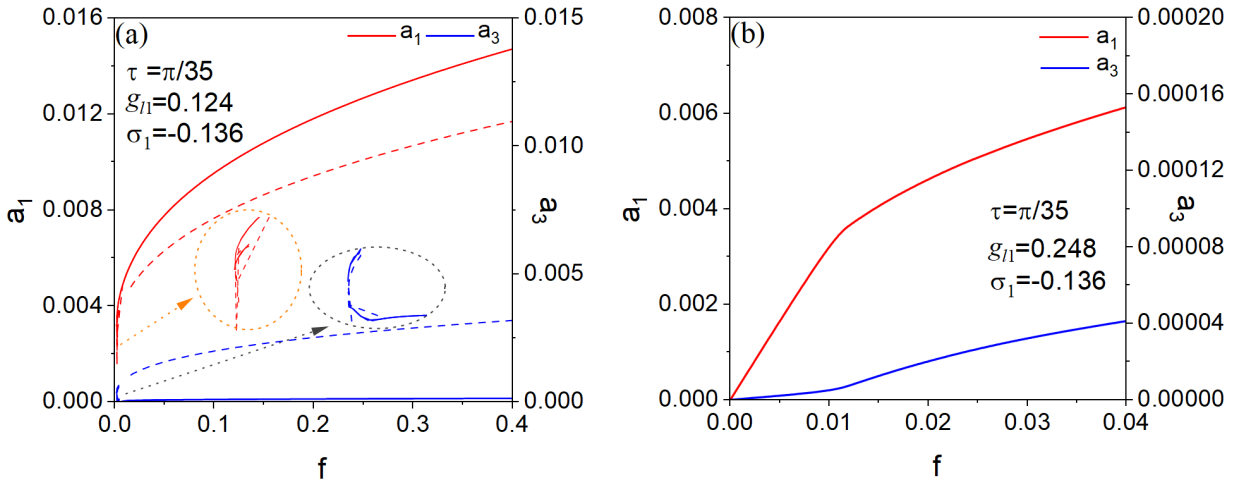

Figure 13: The curves of amplitude versus amplitude of external excitation, $\Omega \approx \omega_1$ ($\sigma_2 = 0$)

References

[1] A. Luongo, G. Rega, F. Vestroni, Monofrequent oscillations of a non-linear model of a suspended cable, J Sound Vib 82 (1982) 247–259.

[2] C. L. Lee, N. Perkins, Nonlinear oscillations of suspended cables containing a two-to-one internal resonance, Nonlinear Dyn 3 (1992) 465–490.

[3] M. Matsumoto, T. Saitoh, M. Kitazawa, H. Shirato, T. Nishizaki, Response characteristics of rain-wind induced vibration of stay-cables of cable-stayed bridges, J Wind Eng Ind Aerod 57 (1995) 323–333.

[4] L. Wang, Y. Zhao, Non-linear planar dynamics of suspended cables investigated by the continuation technique, Eng Struct 29 (2007) 1135–1144.

[5] G. Rao, R. Iyengar, Internal resonance and non-linear response of a cable under periodic excitation, J Sound Vib 149 (1991) 25–41.

[6] G. Rega, W. Lacarbonara, A. Nayfeh, C. Chin, Multiple resonances in suspended cables: direct versus reduced-order models, Int J Non Linear Mech 34 (1999) 901–924.

[7] F. Benedettini, G. Rega, R. Alaggio, Non-linear oscillations of a four-degree-of-freedom model of a suspended cable under multiple internal resonance conditions, J Sound Vib 182 (1995) 775–798.

[8] Y. Zhao, L. Wang, On the symmetric modal interaction of the suspended cable: Three-to-one internal resonance, J Sound Vib 294 (2006) 1073–1093.

[9] N. Srinil, G. Rega, Two-to-one resonant multi-modal dynamics of horizontal/inclined cables. Part II: Internal resonance activation, reduced-order models and nonlinear normal modes, Nonlinear Dyn 48 (2007) 253–274.
[10] N. Srinil, G. Rega, S. Chucheepsakul, Two-to-one resonant multi-modal dynamics of horizontal/inclined cables. Part I: Theoretical formulation and model validation, Nonlinear Dyn 48 (2007) 231–252.
[11] H. Kang, T. Guo, Y. Zhao, W. Fu, L. Wang, Dynamic modeling and in-plane 1:1:1 internal resonance analysis of cable-stayed bridge, Eur J Mech A-solid 62 (2017) 94–109.
[12] Y. Hui, H. Kang, S. Law, Z. Chen, Analysis on two types of internal resonance of a suspended bridge structure with inclined main cables based on its sectional model, Eur J Mech A-solid 72 (2018) 135–147.
[13] L. Xu, Y. Hui, W.-d. Zhu, X. Hua, Three-to-one internal resonance analysis for a suspension bridge with spatial cable through a continuum model, Eur J Mech A-solid 90 (2021) 104354.
[14] Y. Zhao, H. Lin, Nonlinear Dynamics of Suspended Cables under Periodic Excitation in Thermal Environments: Two-to-One Internal Resonance, Int J Bifurc Chaos 31 (2021) 2150153:1–2150153:16.
[15] J. Peng, M. Xiang, L. Wang, X. Xie, H. Sun, J. Yu, Nonlinear primary resonance in vibration control of cable-stayed beam with time delay feedback, Mech Syst and Signal Process 137 (2020) 106488.
[16] X. Su, H. Kang, T. Guo, Modelling and energy transfer in the coupled nonlinear response of a 1:1 internally resonant cable system with a tuned mass damper, Mech Syst and Signal Process 162 (2022) 108058.
[17] C. Sun, Y. Zhao, J. Peng, H. Kang, Y. Zhao, Multiple internal resonances and modal interaction processes of a cable-stayed bridge physical model subjected to an invariant single-excitation, Eng Struct 172 (2018) 938–955.
[18] Q. Wen, X. Hua, X. Lei, Z. Q. Chen, H. Niu, Experimental study of wake-induced instability of coupled parallel hanger ropes for suspension bridges, Eng Struct 167 (2018) 175–187.
[19] L. Chen, Y. Xia, F. Di, G. Zhang, X. Li, T. He, L. Sun, Dynamic modeling and analysis of hanger cables with spacers and dampers for vibration mitigation, Structures 57 (2023) 105209.
[20] J. Ahmad, In-plane linear dynamic behavior and impact of key system parameters of low-sagged cable network, J Sound Vib 490 (2021) 115728.
[21] F. Di, L. Chen, L. Sun, Free vibrations of hybrid cable networks with external dampers and pretensioned cross-ties, Mech Syst and Signal Process 156 (2021) 107627.
[22] C. Xing, H. Wang, A.-q. Li, Y. Xu, Study on Wind-Induced Vibration Control of a Long-Span Cable-Stayed Bridge Using TMD-Type Counterweight, J Bridge Eng 19 (2014) 141–148.
[23] J. Li, J. Shen, S. Zhu, Adaptive self-powered active vibration control to cable structures, Mech Syst and Signal Process 188 (2023) 110050.
[24] Y. Duan, Y. Ni, J. M. Ko, Cable Vibration Control using Magnetorheological Dampers, J Intell Mater Syst Struct 17 (2006) 321 – 325.
[25] Y. Wang, Z. Chen, C. Yang, Z. Liu, J. He, Z. Feng, A novel eddy current damper system for multi-mode high-order vibration control of ultra-long stay cables, Eng Struct 262 (2022) 114319.
[26] N. Olgac, B. Holm-Hansen, A novel active vibration absorption technique: delayed resonator, J Sound Vib 176 (1994) 93–104.
[27] Y. Zhao, J. Xu, Effects of delayed feedback control on nonlinear vibration absorber system, Journal of Sound and Vibration 308 (2007) 212–230.
[28] J. Peng, L. Wang, Y. Zhao, S. Lenci, Time-delay dynamics of the mr damper-cable system with one-to-one internal resonances, Nonlinear Dyn 105 (2021) 1343 – 1356.
[29] Y. Liu, N. Olgac, L. Cheng, Delayed resonator with multiple distributed delays–considering and optimizing the inherent loop delay, J Sound Vib 576 (2024) 118290.
[30] Y. Zhao, C. Sun, Z. Wang, J. Peng, Nonlinear in-plane free oscillations of suspended cable investigated by homotopy analysis method, Struct Eng Mech 50 (2014) 487–500.
[31] L. Wang, Y. Zhao, Nonlinear interactions and chaotic dynamics of suspended cables with three-to-one internal resonances, Int J Solids Struct 43 (2006) 7800–7819.
[32] H. Lin, Y. Zhao, P. Zheng, X. Wu, X. Zhang, Modal coupled vibration characteristics of suspended cables with temperature condition, Chin J Appl Mech 40 (2023).